PHYSICAL REVIEW B **70**, 161404(R) (2004)

# Three-pulse photon-echo spectroscopy as a probe of the photoexcited electronic state manifold in coupled electron-phonon systems

A. Piryatinski,* S. Tretiak, P. W. Fenimore, A. Saxena, R. L. Martin, and A. R. Bishop
*Theoretical Division, Center for Nonlinear Studies, MS B258, Los Alamos National Laboratory, Los Alamos, New Mexico 87545, USA*

(Received 10 August 2004; published 29 October 2004)

We demonstrate that a three-pulse photon-echo technique is capable of eliminating the effect of the absorption band broadening associated with *intrinsic* electron-phonon coupling, and revealing its structure determined by the optical transitions between the ground and excited electronic states dressed with vibrational quanta. This is important for the spectroscopic probing of photoexcited dynamics in low-dimensional materials with strong electron-phonon coupling. As a minimal model for our calculations, we use a two-electron, two-site Holstein Hamiltonian accounting for the vibrational degree of freedom fully quantum mechanically.

DOI: 10.1103/PhysRevB.70.161404 PACS number(s): 78.47.+p, 82.53.Kp

Photon-echo techniques are reliable tools for eliminating inhomogeneous broadening effects on the time-resolved signal decay and revealing hidden dynamical information.[1,2] The origin of inhomogeneous broadening lies in a random distribution of transition energies in the ensemble of optically active centers in solids or molecules in solution. Usually, such a distribution originates from the effect of the environment, e.g., static energy disorder in glasses, conformational disorder of solvated (bio)polymers, and/or "slow" fluctuations in liquids. In this communication we demonstrate that a three-pulse photon-echo (3PE) technique is also capable of eliminating the effect of the absorption band broadening associated with *intrinsic* electron-phonon coupling. The existence of such an effect does not depend on a specific electron-phonon coupling scheme. A model adopted here will be used to identify ranges of parameters suggesting which compounds from a broad class of low-dimensional materials might demonstrate this effect.

It is well understood that electron-phonon interactions strongly influence the electronic dynamics in low-dimensional materials such as (bio)polymers,[3–5] biological complexes,[6,7] mixed-valence complexes,[8,9] etc. Photoexcited dynamical aspects such as exciton and breather (multiquanta bound state) formation, internal dynamics, transport, photochemical reactions, and charge transfer are currently investigated.[4,10–12] Theoretically, the issue of treating vibrational degrees of freedom quantum mechanically so as to study the nonadiabatic electronic dynamics is of great interest. Experimentally, the complexity and ultrafast nature of the dynamics require the use of state-of-the-art time- and/or frequency-resolved optical techniques.[4] Unambiguous identification of desirable dynamical and structural features in the optical and infrared signals relies on accurate theoretical modeling of the dynamics and optical properties.[13–18]

As a minimal model to describe the coupled electron-phonon system, we use a two-site Holstein Hamiltonian,

$$H = -t_0 \sum_{\sigma} (c_{1\sigma}^{\dagger} c_{2\sigma} + c_{2\sigma}^{\dagger} c_{1\sigma}) + \frac{\lambda}{\sqrt{2\omega_0}} \sum_{i=1,2} \sum_{\sigma} (a_i^{\dagger} + a_i) n_{i\sigma} + \omega_0 \sum_i \left( a_i^{\dagger} a_i + \frac{1}{2} \right), \quad (1)$$

which is a limiting case of the general half-filled electronic band model. Here $c_{i\sigma}^{\dagger}$ and $c_{i\sigma}$ ($a_i^{\dagger}$ and $a_i$) are electron (phonon) creation and annihilation operators on site $i$ with spin projection $\sigma$; $n_{j\sigma}=c_{j\sigma}^{\dagger}c_{j\sigma}$ is the electron state population operator; and $t_0$ is electron transfer energy. The electron-phonon coupling constant is $\lambda$, and the bare phonon energy is $\omega_0$. In the electronic basis set $\{|\uparrow_1\downarrow_2\rangle \pm |\uparrow_2\downarrow_1\rangle; |\uparrow_1\downarrow_1\rangle \pm |\downarrow_2\uparrow_2\rangle; |\downarrow_1\downarrow_2\rangle; |\uparrow_1\uparrow_2\rangle\}$, the problem effectively reduces to a *three-level* electronic system of spin-singlet states. The spin-triplet states $\{|\downarrow_1\downarrow_2\rangle; |\uparrow_1\downarrow_2\rangle - |\uparrow_2\downarrow_1\rangle; |\uparrow_1\uparrow_2\rangle\}$ decouple since no spin-orbit interaction is present. The spin-singlet states are coupled via a single vibrational mode $a=a_1-a_2$. The center-of-mass motion is decoupled due to the dimer inversion symmetry. For further analysis we will use the following dimensionless units: total energy $\bar{\varepsilon}=E/(\sqrt{2}t_0)$, electron-phonon coupling energy $\bar{\lambda}=\lambda/(t_0\sqrt{\omega_0})$, bare phonon energy $\bar{\omega_0}=\omega_0/(\sqrt{2}t_0)$, vibrational displacement $\bar{\xi}=\sqrt{2\omega_0}q$, where $q$ is the displacement in the length units, and time $\bar{t}=\sqrt{2}t_0 t$, where $t$ has time dimensionality.

Using a Lanczos algorithm, we diagonalized the Hamiltonian (1) for fixed $\bar{\omega_0}=0.24$, and electron-phonon coupling varying in the range $\bar{\lambda}=0.0$–$1.0$. The phase diagram representing the spectrum as a function of $\bar{\lambda}$ is shown in Fig. 1. We distinguish three regions: (i) a low-energy region, where the spacing between the electronic eigenenergies reduces exponentially as $\bar{\lambda}$ increases, indicating the formation of a double-well barrier; (ii) a high-energy region, where levels undergo avoided crossing, and nonadiabatic effects are significant; and (iii) the ground state double-well region where the levels are twofold degenerate and equally spaced.

In this communication, we focus on the manifold of the *photoexcited* eigenstates by defining the dipole moment operator as

$$\hat{\mu} = \mu_{12}(c_1^{\dagger}c_2 + c_2^{\dagger}c_1) + \mu_0(n_2 - n_1) + \delta\mu(a^{\dagger} + a)(n_2 - n_1), \quad (2)$$

where $\mu_{12}$ is the transition dipole due to the charge transfer between the sites 1 and 2. $\mu_0$ is the dipole matrix element representing a positive nucleus charge on one ionized site and negative electron charge promoted to the other site, and $\delta\mu$ is the additional contribution to the second term due to

 

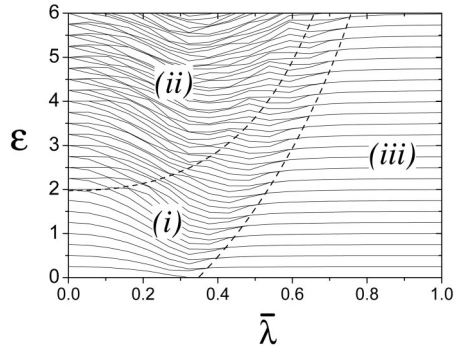


FIG. 1. Phase diagram: energy eigenvalues $\varepsilon$ vs the strength of electron-phonon coupling. Region (i) is a single-well ground electronic state. (ii) Excited-state avoided crossing region accessible through photoexcitations. (iii) Double-well (twofold energy degenerate) electronic ground-state region.

the linear displacements of the charges from the average positions. Since it does not matter for our further consideration if any of them dominates, we set all of them to unity. The linear absorption line shape is then determined by the overlap of the distribution functions of the bound bare vibrational quanta in the ground and the photoexcited states, since the first two terms in Eq. (2) act only on the electronic components of the wave functions. The third term corresponds to an additional contribution due to the overlap of the ground-state distribution whose center is shifted to ±1 and the excited state. Provided both distributions are broad, i.e., the electronic states are heavily dressed, then the third term corresponds to the same overlap integral as the first two.

The absorption spectra for $\bar{\lambda}=0.27$ and $\bar{\lambda}=1.0$ are shown in Figs. 2(a) and 2(b), respectively. For $\bar{\lambda}=0.27$ the transition takes place from the ground state in region (i) of Fig. 1 described by the flat adiabatic curve shown in Fig. 2(c). For $\bar{\lambda}=1.0$ it starts in region (iii) of Fig. 1 described by the double well in Fig. 2(d). Both transitions take place in region (ii) of Fig. 1 (for $\bar{\lambda}=1.0$ it lies in the high-energy range not shown in the plot but has the same structure as the one shown). Comparing the excited-state vibrational quanta distribution functions (not shown in the plot), we have found that in both cases it is broad. As a result, the absorption lineshape, i.e., the overlap, is simply the ground-state distribution function. The spectrum in Fig. 2(a) has a progression of several absorption lines associated with few coupled vibrational quanta. Increasing $\bar{\lambda}$ leads to increasing the number of bound vibrational quanta. For $\bar{\lambda}=1.0$ the ground state is at the minimum of the double-well potential [Figs. 1 and 2(d)], and the vibrational component of the wave function is a coherent state, i.e., a Gaussian distribution with $\langle n\rangle=2\bar{\lambda}^2/\bar{\omega}_0^3=74$ and $\sigma_n=\sqrt{\langle n\rangle}=8.6$. Therefore, the absorption spectrum shown in Fig. 2(b) contains a large number of lines under the Gaussian envelope.

Provided the homogeneous widths of the lines within the band in Fig. 2(b) are larger than the energy spacing between them, the spectrum becomes dense. This case is represented in Fig. 2(b) by the envelope band, where we set the homo-

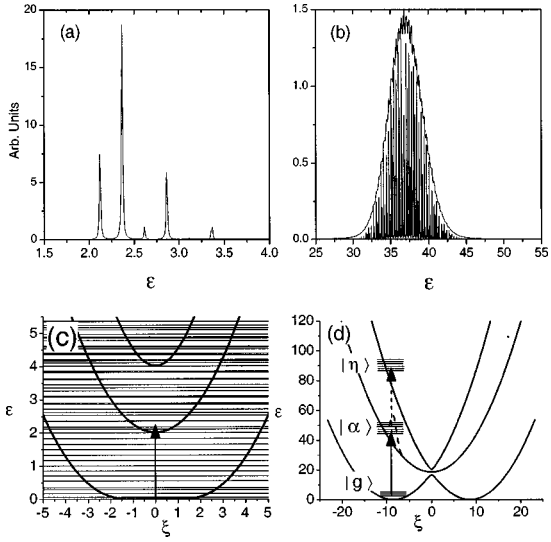


FIG. 2. Linear absorption spectra for (a) $\bar{\lambda}=0.27$ and (b) $\bar{\lambda}=1.0$, where the envelope is the spectrum calculated for large $\gamma=0.17$ homogeneous broadening. Optical transitions $|g\rangle\rightarrow|\alpha\rangle$ corresponding to the spectra in (a) and (b) are shown in the adiabatic potential-energy diagrams (c) and (d), respectively.

geneous linewidth $\gamma=0.17$. (Here and below, $\gamma$ has the same dimensionless units as $\varepsilon$.) Consequently, no valuable structural and dynamical information can be obtained from the linear spectra associated with the optical transition from region (iii) to (ii) in Fig. 1 under such conditions. In this communication we demonstrate that it is possible to use the nonlinear 3PE technique to resolve the fine structure of the band, something which cannot be achieved using the two-pulse photon-echo (2PE) technique.

The 3PE technique involves a sequence of three light pulses separated by delay times $t_1$ and $t_2$, as shown in Fig. 3(a). The polarization excited by the pulse train is observed in the direction determined by the wave vector $\mathbf{k}_s$, satisfying the phase-matching conditions shown in Fig. 3(a). The first pulse excites coherences between the ground and the first excited state manifolds shown in Fig. 2(d). These coherences (i.e., off-diagonal components of the nonequilibrium density matrix) propagate during the delay time $t_1$ [diagrams 1–3 in Fig. 3(b)]. The second pulse reexcites the ground state (diagram 1) and the first (diagrams 2, 3) electronic excited state populations (i.e., the diagonal components of the density matrix). Since the excited state and the ground-state manifolds are described by the number of eigenstates associated with the bound vibrational quanta, then, in addition to the populations, the excited and the ground-state coherences are excited. The populations and coherence dynamics propagating during the "population" time $t_2$ are described by the irreducible parts in the density-matrix equation, which account for the fast environmental fluctuations,[2] and are shown as shaded boxes in Fig. 3(b). The third pulse reexcites the coherence between the ground state and the first excited electronic state manifolds [Fig. 2(d) and diagrams 1 and 2 in Fig. 3(b)], as well as between the first and the second excited state manifolds [see Fig. 2(d) and diagram 3 in Fig. 3(b)] further evolving during time $t_3$. The total polarization excited by the pulse

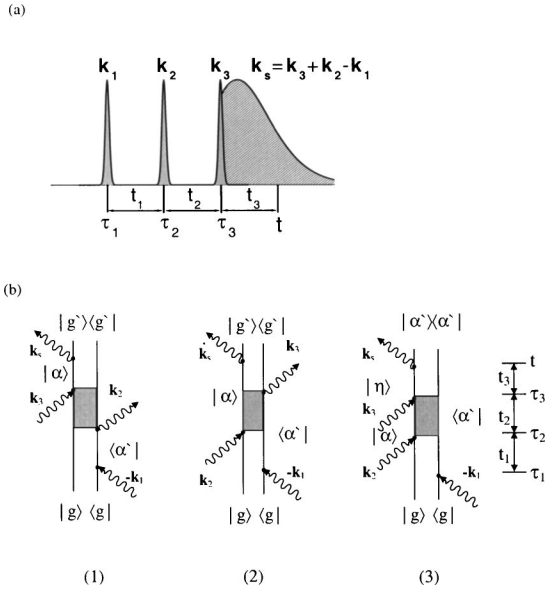


FIG. 3. (a) Schematic diagram of a three-pulse echo sequence and the signal generated in the direction $\mathbf{k_s}=\mathbf{k_3}+\mathbf{k_2}-\mathbf{k_1}$. (b) Double-sided Feynman diagrams describing all contributions to the 3PE signal for the three-band system in the rotating wave approximation. The three-band scheme, $|g\rangle$, $|\alpha\rangle$, and $|\eta\rangle$ is shown in Fig. 2(d).

train is a superposition of these three diagrams, each corresponding to the following third-order response function components[2,16]

$$R_n^{(3)} = i\sum_{g,g'}\sum_{\alpha,\alpha'} \mu_{g\alpha'}\mu_{\alpha' g'}\mu_{g\alpha}\mu_{\alpha g'} e^{(i\bar{\omega}_{\alpha' g}-\gamma_{g\alpha'})\bar{t}_1-(i\bar{\omega}_{\alpha g'}+\gamma_{g\alpha'})\bar{t}_3} \times [\delta_{1,n} e^{-(i\bar{\omega}_{gg'}+\Gamma_{gg',gg'})\bar{t}_2} + \delta_{2,n} e^{-(i\bar{\omega}_{\alpha\alpha'}+\Gamma_{\alpha\alpha',\alpha\alpha'})\bar{t}_2}], \quad n=1,2; \tag{3}$$

$$R_3^{(3)} = -i\sum_{g,\eta}\sum_{\alpha,\alpha'} \mu_{g\alpha}\mu_{\alpha\eta}\mu_{\eta\alpha'}\mu_{\alpha' g} \times e^{(i\bar{\omega}_{\alpha' g}-\gamma_{g\alpha'})\bar{t}_1-(i\bar{\omega}_{\alpha\alpha'}+\Gamma_{\alpha\alpha',\alpha\alpha'})\bar{t}_2-(i\bar{\omega}_{\eta\alpha'}+\gamma_{\eta\alpha'})\bar{t}_3}, \tag{4}$$

where $\gamma_{g\alpha'}$ is the homogeneous dephasing rate between the electronic ground and excited states; $\Gamma_{\alpha\alpha',\alpha\alpha'}$ $(\alpha\neq\alpha')$ and $\Gamma_{gg',gg'}$ $(g\neq g')$ are relaxation tensor components describing the excited and the ground state dephasing rates. Here we neglect the ground and excited state population relaxation processes, since they occur on time scales longer than the dephasing.[2] Here we assume the homodyne time-gated detection given by $S(\bar{t}_3,\bar{t}_2,\bar{t}_1)\propto|\Sigma_{i=1,2,3}R_i^{(3)}(\bar{t}_3,\bar{t}_2,\bar{t}_1)|^2$ (Refs. 2 and 16). The delay time $\bar{t}_3$ in this mode denotes the time after the third pulse arrives and the time-gated measurement of the signal intensity is performed.

Although the absorption band in Fig. 2(b) is formed from a number of homogeneously broadened lines, it cannot be considered as an inhomogeneously broadened band, since its structure is induced by the interaction with a phonon mode, and not by the bath degrees of freedom (continuum of modes). Accordingly, for the 2PE we set $\bar{t}_2=0$ in Eqs. (3), and assume that $\gamma_{g\alpha'}=\gamma$ for any $\alpha$, $g$, as well as using a Gaussian distribution for the oscillator strength $\mu_{g\alpha}\mu_{\alpha g'}\propto\exp[-(\omega_{\alpha,g}-\omega_0)^2/2\sigma^2]$ [see Fig. 2(b)]. The optical transitions originate from the lowest vibrational state $g$ in the electronic ground state. This is the case for the high-energy vibrational modes ($>300\ \mathrm{cm}^{-1}$) at room temperature. After averaging the response function over the oscillator strength distribution, one finds that $R_{1,2}^{(3)}\propto\exp[-(\sigma^2\bar{t}_1^2+\sigma^2\bar{t}_3^2)/2-\gamma(\bar{t}_1+\bar{t}_3)]$. The other component [Eq. (4)] will have a similar structure. If the widths of the absorption band $\sigma>\gamma$, then the nonlinear signal experiences free-induction decay (FID) on a time scale of $1/\sigma$, similar to the linear signal decay.

However, if $1/\Gamma_{\alpha\alpha',\alpha\alpha'}<\bar{t}_2$ the off-diagonal components $|\alpha\rangle\langle\alpha'|$ of the density matrix in diagrams 1–3 (Fig. 3) vanish. Further averaging of Eq. (3), $n=2$, with the transition oscillator strength distribution corresponds to $R_2^{(3)}\propto\exp[-\sigma^2(\bar{t}_1-\bar{t}_3)^2-\gamma(\bar{t}_1+\bar{t}_3)]$. This term is equivalent to that describing the response of a two-level system with the inhomogeneously distributed transition energies. As a result it corresponds to the "photon-echo" signal whose peak decay at $\bar{t}_1=\bar{t}_3$ is determined by $\gamma$, i.e., the inverse width of the homogeneously broadened lines forming the band, e.g., in Fig. 2(b). We note that, in contrast to the inhomogeneous broadening case, the echo appears only due to the second component of the response function [Eq. (3), $n=2$]; the other will still be experiencing the FID. Consequently, the echo signal becomes sensitive to the processes solely within the first excited state manifold, offering a *unique probe* of the photoexcited dynamics.

We have calculated the 3PE time-gated signal for different delay times $\bar{t}_2$ using Eqs. (3) and (4), where the eigenenergies and eigenstates were calculated by direct diagonalization of the Hamiltonian (1). For simplicity we set all excited (ground) state dephasing rates to $\Gamma_{\alpha\alpha',\alpha\alpha'}=1/T_e^*$ $(\Gamma_{gg',gg'}=1/T_g^*)$, where $T_e^*=0.24$ $(T_g^*=0.24)$ is the excited (ground) state dephasing time. The dephasing *between* the ground and excited states was set to $\gamma=0.17$, the same as corresponding to the envelope band in Fig. 2(b).

A two-dimensional (2D) $(\bar{t}_1,\bar{t}_3)$ 3PE signal plot is shown in Fig. 4. The inset in panel (a) presents the $\bar{t}_1=\bar{t}_3$ slice of the signal in both panels on the log scale. In the 2D plot the presence of the "photon-echo" effect, i.e., signal maximum at $\bar{t}_1=\bar{t}_3$, would appear as a signal stretched along the diagonal $\bar{t}_1=\bar{t}_3$. As one can see in panel (a) representing the 2PE $(\bar{t}_2=0)$ response and in the inset, the signal decays rapidly and there is no well-defined diagonal, "photon-echo," component. In contrast, in panel (b), where a 3PE signal for $\bar{t}_2>T_e^*$ $(\bar{t}_2=1.2)$ is shown, there is a diagonal $(\bar{t}_1=\bar{t}_3)$ "photon-echo" component. The echo decay is seen in the inset as the exponential component at $\bar{t}>5$. The signal in panel (b) contains information on two different time scales. Its width describes the FID time scale, whereas its diagonal length is $\sim\gamma$. In this sense, the photon echo allows us to resolve the internal "hidden" structure of the line shape. This result is important, since the dynamics of different spectral components of a photoexcited wave packet could be resolved using a 3PE technique.

We expect the technique proposed here to have broad ap-

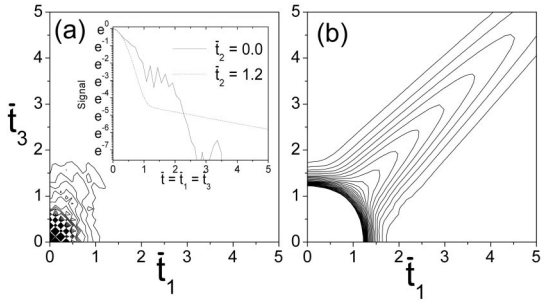


FIG. 4. Contour plot of the 3PE signal: (a) Populations delay time $\bar{t}_2=0$ is smaller than the ground and excited state dephasing times $T_g^*=T_e=0.24$; no echo signal is seen along the diagonal $\bar{t}_1=\bar{t}_3$. (b) Populations delay time $\bar{t}_2=1.2$ is larger than the ground and excited state dephasing times $T_g^*=T_e$; echo signal is clearly seen along the diagonal $\bar{t}_1=\bar{t}_3$. The inset to (a) shows $\bar{t}_1=\bar{t}_3$ slices of (a) and (b).

plications. Observation of the discussed 3PE effect requires that the following two conditions are satisfied: (a) the ground and the photoexcited states should be strongly dressed with vibrational quanta [e.g., lie in the regions (iii) and (ii) in Fig. 1, respectively, for the adopted model]; and (b) fast dephasing within the excited-state manifold compared to the population decay must occur. Also note that if we add to the Hamiltonian (1) small on-site Coulomb interaction (Holstein–Hubbard model), $U<\lambda/(2\sqrt{\omega_0})$, it would change the shape of the adiabatic surfaces near the crossing points in Fig. 2(d), but will have little effect on the number of the bound vibrational quanta. Therefore, no changes in the photon echo should be observed as shown in Ref. 22. One interesting material prospect is the recently synthesized two-electron mixed-valence molecular complex,[19,20] where the metal centers can be described as Ir(0)-Ir(II). Examples in solids include strong charge-density-wave systems such as Wolfram's Red Salt, a Pt(II)-Pt(IV) system, extensively studied by Raman techniques.[9] In a related area, the proposed technique could be used to probe low-frequency vibrational wave-packet dynamics strongly coupled to high-frequency vibrations, e.g., O-H stretch,[21] rather than to electronic degrees of freedom.

To conclude, using a two-electron, two-site Holstein model to describe a photoexcited coupled electron-phonon state manifold, we have demonstrated that the 3PE technique can be used to resolve dense excited-state bands intrinsically associated with strong electron-phonon coupling. Additionally, the photon-echo response is able to resolve the complexity of the time scales associated with the inhomogeneous broadening of the spectra by utilizing the 2PE response, as well as the complex structure of the absorption band dynamically induced through the electron-phonon coupling (3PE). This suggests the possibility of experiments directly probing the photoexcited dynamics in a variety of materials with strong electron-phonon coupling. Furthermore, details of the complex time scales within the excited-state manifold can be resolved using multidimensional heterodyned Fourier-transformed echo techniques.[16]

Work at LANL is supported by the the Center for Nonlinear Studies and the LDRD program of the U.S. Department of Energy. We would like to thank Andy P. Shreve for discussing with us feasible experimental verification of the reported effect. A.P. is indebted to Eugene Tsiper for stimulating discussions.

*Corresponding author. Email address: apiryat@lanl.gov

[1] L. Allen and J. Eberly, *Optical Resonance and Two-Level Atoms* (Dover, New York, 1987).
[2] S. Mukamel, *Principles of Nonlinear Optical Spectroscopy* (Oxford University Press, Oxford, 1995).
[3] A. Xie *et al.*, Phys. Rev. Lett. **84**, 5435 (2000).
[4] S. Adachi, V. M. Kobryanskii, and T. Kobayashi, Phys. Rev. Lett. **89**, 027401 (2002).
[5] S. Tretiak *et al.*, Phys. Rev. Lett. **89**, 097402 (2002).
[6] Y. Mizutani and T. Kitagawa, Science **278**, 443 (1997).
[7] M. C. Simpson *et al.*, J. Am. Chem. Soc. **119**, 5110 (1997).
[8] J. T. Gammel *et al.*, Phys. Rev. B **45**, 6408 (1992).
[9] K. Prassides *et al.*, J. Phys. Chem. **90**, 1978 (1986).
[10] A. R. Bishop *et al.*, Phys. Rev. Lett. **52**, 671 (1984).
[11] W. Z. Wang *et al.*, Phys. Rev. Lett. **80**, 3284 (1998).
[12] S. Tretiak *et al.*, Proc. Natl. Acad. Sci. U.S.A. **100**, 2185 (2003).
[13] S. Mukamel, Annu. Rev. Phys. Chem. **51**, 691 (2000).
[14] P. Hamm and R. M. Hochstrasser, in *Ultrafast Infrared and Raman Spectroscopy*, edited by M. D. Fayer (Dekker, New York, 2001), p. 273.
[15] K. A. Merchant, D. E. Thompson, and M. D. Fayer, Phys. Rev. Lett. **86**, 3899 (2001).
[16] A. Piryatinski, V. Chernyak, and S. Mukamel, in *Ultrafast Infrared and Raman Spectroscopy* (Ref. 14), p. 349.
[17] A. Piryatinski, C. P. Lawrence, and J. L. Skinner, J. Chem. Phys. **118**, 9672 (2003).
[18] C. J. Fecko *et al.*, Science **301**, 1698 (2003).
[19] A. F. Heyduk and D. G. Nocera, Chem. Commun. (Cambridge) **1999**, 1519 (1999).
[20] A. F. Heyduk and D. G. Nocera, J. Am. Chem. Soc. **122**, 9415 (2000).
[21] N. Huse *et al.*, Phys. Rev. Lett. **91**, 197401 (2003).
[22] See EPAPS Document No. E-PRBMDO-70-R08440 for a contour plot of 3PE with the same parameters as in Fig. 4 except $U/t_0=0.3$. A direct link to this document may be found in the online article's HTML reference section. The document may also be reached via the EPAPS homepage (http://www.aip.org/pubservs/epaps.html) or from ftp.aip.org in the directory /epaps/. See the EPAPS homepage for more information.